nature communications

Article

https://doi.org/10.1038/s41467-025-67695-4

CO_2 hydrogenation toward toluene methylation for selective para-xylene synthesis

Received: 31 August 2025

Accepted: 5 December 2025

Published online: 24 December 2025

Check for updates

Junqi Tian[1,2,6], Yongjie Xi[3,6], Jianian Cheng[1,2], Jieyun Zhang[1,2], Hao Wang[1,2], Fujun Ren[1,2], Jun Yuan[1,2], Changxin He[1,2], Hongfang Yang[1,2], Chengyuan Liu[4], Zelong Li[1,2,3] ✉ & Can Li[1,2,5] ✉

The selective production of high-value para-xylene (PX) through CO_2 hydrogenation-coupled toluene methylation represents a promising strategy for sustainable carbon utilization. Herein, we report a $ZnZrO_x$ & HMCM-22 tandem catalyst that integrates CO_2 hydrogenation with shape-selective toluene methylation. The optimized catalyst achieves 91% xylene selectivity with 70.4% PX dominance at 10.3% toluene conversion. Controlled tetraethyl orthosilicate (TEOS) deposition passivates Brønsted acid sites in HMCM-22 supercages, suppressing toluene disproportionation while preserving methylation activity in sinusoidal channels. Mechanistic studies reveal that formaldehyde species, generated on $ZnZrO_x$ and transferred to HMCM-22, act as kinetically favored methylating intermediates, enabling direct coupling between CO_2 hydrogenation and toluene methylation. This pathway outperforms conventional methanol-mediated routes in both activity and selectivity. Our work establishes a dual-optimization strategy—zeolite microenvironment engineering and reactive intermediate control—offering mechanistic insights and design principles for high-performance tandem catalysis in carbon recycling aromatic synthesis.

Carbon dioxide, as an abundant C1 feedstock, presents a great opportunity for sustainable chemical synthesis when coupled with green hydrogen derived from renewable energy. Recent advances have demonstrated the feasibility of converting CO_2/H_2 mixtures into value-added products including methanol[1,2], light olefins[3–6], and aromatics[7–9]. Although direct CO_2 hydrogenation to aromatics has been reported using tandem catalysis, the para-xylene (PX) selectivity within aromatic products remains suboptimal. This limitation contrasts sharply with the industrial demand for PX—a precursor for polyethylene terephthalate (PET) manufacturing—which currently relies predominantly on fossil-based routes such as naphtha cracking and methanol-mediated toluene alkylation. These considerations highlight the urgency to develop efficient strategies for synthesizing PX through CO_2-derived methylating agents with toluene, thereby enabling PX production via a two-step CO_2/H_2 pathway.

Conventional toluene methylation processes employing methanol confront intrinsic thermodynamic limitations when implemented over H-ZSM-5 zeolites at 400–500 °C. Under these harsh thermal conditions, the concurrent activation of methanol-to-olefins (MTO) side reactions precipitates a cascade of operational challenges:

[1]Key Laboratory of advanced catalysis, College of Chemistry and Chemical Engineering, Lanzhou University, Lanzhou, China. [2]State Key Laboratory of Natural Product Chemistry, College of Chemistry and Chemical Engineering, Lanzhou University, Lanzhou, Gansu, China. [3]State Key Laboratory of Low Carbon Catalysis and Carbon Dioxide Utilization, Lanzhou Institute of Chemical Physics, Chinese Academy of Sciences, Lanzhou, China. [4]National Synchrotron Radiation Laboratory, University of Science and Technology of China, Hefei, China. [5]State Key Laboratory of Catalysis, Dalian Institute of Chemical Physics, Chinese Academy of Sciences, Dalian National Laboratory for Clean Energy, Dalian, Liaoning, China. [6]These authors contributed equally: Junqi Tian, Yongjie Xi. ✉e-mail: lizl@lzu.edu.cn; canli@dicp.ac.cn

competitive methanol consumption by olefin synthesis pathways leads to methylating agent depletion, while concomitant carbon deposition accelerates catalyst deactivation through pore blockage and active site coverage[10,11]. Furthermore, the kinetic rivalry between methylation and MTO pathways severely compromises reaction efficiency. This tripartite interplay of resource misallocation, catalyst instability, and suppressed target reaction kinetics collectively necessitates the development of catalytic architectures capable of circumventing methanol intermediation under thermodynamically favorable conditions.

Recent developments in tandem catalysis reveal promising alternatives through in situ-generated oxygenate intermediates. Oxide-zeolite composites (e.g., oxide: $ZnZrO_x$, $ZnGa_2O_4$, In_2O_3-ZrO_2, $ZnCrO_x$; zeolites: SAPO-34, SSZ-13, H-ZSM-5)[12–16] enable CO_2 hydrogenation to lower olefins and aromatics via CH_xO intermediates through formate-mediated pathways. Notably, these systems operate at significantly lower temperatures than conventional methanol-based processes, as CH_xO intermediates exhibit lower activation barriers compared to free methanol. Our previous work further demonstrated that methanol synthesis in tandem systems is thermodynamically driven by downstream olefin formation—a critical coupling mechanism that facilitates intermediate-directed catalysis[4]. These findings suggest that judicious selection of reactive methylating intermediates could decouple methylation kinetics from MTO side reactions.

Emerging CO_2 hydrogenation-coupled toluene methylation strategies underscore the pivotal influence of zeolite architectural design on product selectivity[17–20]. Whereas H-ZSM-5-based systems deliver moderate xylene yields, their inherent structural constraints—notably unidirectional channel geometry and pronounced Brønsted acidity—predispose the system toward competing toluene disproportionation and xylene isomerization pathways[21,22]. In contrast, MCM-22 zeolite demonstrates distinctive structural merits for shape-selective alkylation, characterized by sinusoidal 10-membered ring (10-MR) channels that impose steric restrictions on bulkier isomers, coupled with chemically tunable supercage configurations enabling precise acid site modulation. The spatial isolation of active sites within this architecture further suppresses disproportionation side reactions. These collective structural attributes establish MCM-22 as an exemplary scaffold for constructing tailored methylation microenvironments with enhanced selectivity[23,24].

In this work, we develop a bifunctional $ZnZrO_x$ & HMCM-22 (ZZO & M-22) tandem catalyst that synergistically integrates CO_2 hydrogenation and shape-selective methylation. Through strategic silica deposition in MCM-22 supercages, we selectively passivate Brønsted acid sites responsible for toluene disproportionation while preserving methylation-active sites in sinusoidal channels. Experimental results, advanced characterization via in situ synchrotron vacuum ultraviolet photoionization mass spectrometry (SVUV-PIMS) and density functional theory (DFT) calculations identify formaldehyde-like CH_2O^* as the dominant methylating intermediate, exhibiting a 0.86 eV lower activation barrier compared to methanol-mediated pathways. The optimized catalyst achieves 91% xylene selectivity with 70.4% PX dominance among isomers at 10.3% toluene conversion. This study establishes a dual-optimization strategy combining zeolite microenvironment engineering with reactive intermediate control, providing a blueprint for developing industrially viable CO_2-to-aromatics systems.

Results and discussion

Catalytic performance

The catalytic performance of tandem catalyst systems was systematically investigated in a fixed-bed reactor under controlled reaction conditions. Temperature-dependent studies show a monotonic increase in toluene conversion from 3% to 32% with simultaneous attenuation of PX selectivity with increasing reaction temperature from 280 to 400 °C (Fig. 1a, and Supplementary Fig. 1a). Thermodynamic redistribution of xylene isomers favored meta-xylene (MX) formation, accompanied by decreasing benzene selectivity and progressive accumulation of 1,2,4-trimethylbenzene (TMB) with increasing reaction temperature. This temperature-response profile suggests competing mechanisms: enhanced alkylation kinetics promoting active methyl species-toluene coupling at elevated temperatures, versus thermally activated processes including xylene isomerization to MX and over-methylation to TMB. Comparative evaluation of individual components in the ZZO & M-22 tandem system demonstrated distinct functionalities ZZO exclusively mediated CO_2-to-methanol conversion while M-22 remained catalytically inert in isolation for CO_2 hydrogenation (Fig. 1b). The combined system achieved integrated CO_2 hydrogenation and toluene methylation without generating aromatization byproducts, with control experiments confirming toluene disproportionation as the dominant pathway on isolated M-22 with toluene as feedstocks.

Modification of M-22 via tetraethyl orthosilicate (TEOS) deposition induced three critical effects: pore architecture modulation favoring PX diffusion, passivation of external acidic sites, and suppression of disproportionation pathways. Progressive TEOS deposition cycles (1–4 cycles) enhanced PX selectivity from 43% to 64% while suppressing benzene selectivity from 10% to <1%, though with concomitant TMB accumulation (9%) due to restricted PX diffusion enabling secondary methylation (Fig. 1c). Five deposition cycles induced pore blockage, manifesting as activity loss with toluene conversion decreasing from 14% to 7%, establishing 4-cycle modification (ZZO & 4Si/M-22) as the optimal configuration. The ZZO & 4Si/M-22 catalyst achieves 91% xylene selectivity with 70.4% PX dominance among isomers at 10.3% toluene conversion. Compared to other catalyst systems, the ZZO & 4Si/M-22 can obtain a high xylene selectivity while achieving a high PX selectivity, and can completely inhibit the occurrence of toluene disproportionation side reactions (Supplementary Table 1). And the ZZO & 4Si/M-22 achieved a CO_2 conversion of 4.2% with a CO selectivity of 22% at 320 °C (Supplementary Fig. 1b). Long-term stability tests confirmed sustained performance (>120 h) with undiminished PX selectivity (Fig. 1d).

Process parameter optimization revealed pressure-dependent behavior with elevated pressure from 1 to 6 MPa, which enhances toluene conversion from 5% to 12% but promotes TMB formation with selectivity increasing from 4% to 12% through PX retention-induced over-methylation (Supplementary Fig. 2a). Gas hourly space velocity (GHSV) studies identified 12,000 mL g^{-1} h^{-1} as optimal, balancing toluene conversion (10.3%) and selectivity (PX 64%, TMB 9%), with lower GHSV to 6,000 mL g^{-1} h^{-1} inducing disproportionation pathways (Supplementary Fig. 2b). Weight hourly space velocity (WHSV) adjustments demonstrated an intrinsic activity-selectivity trade-off: increasing WHSV from 1 to 3 h^{-1} improved PX selectivity from 64 to 80% but incurred 80% toluene conversion loss with decreasing from 10.3% to 2%, while simultaneously suppressing TMB formation (Supplementary Fig. 2c). These systematic investigations establish the ZZO & 4Si/M-22 system as an effective tandem catalyst for selective PX production, achieving precise control through synergistic component integration, strategic pore engineering, and optimized reaction parameters.

Structure characterization of the tandem catalysts

The ZZO solid solution oxide catalyst was synthesized through 20 mol% ZnO doping into ZrO_2. X-ray diffraction analysis confirms that the resultant ZZO solid solution adopts a characteristic tetragonal crystal structure, as evidenced by the diffraction pattern in Fig. 2a. As shown in the transmission electron microscopy (TEM) image (Fig. 2b), the ZZO material exhibits a nanoparticle morphology with uniform dimensions. Elemental mapping analysis further demonstrates the homogeneous distribution of Zn atoms within the ZrO_2 matrix (Fig. 2c), verifying the

https://doi.org/10.1038/s41467-025-67695-4

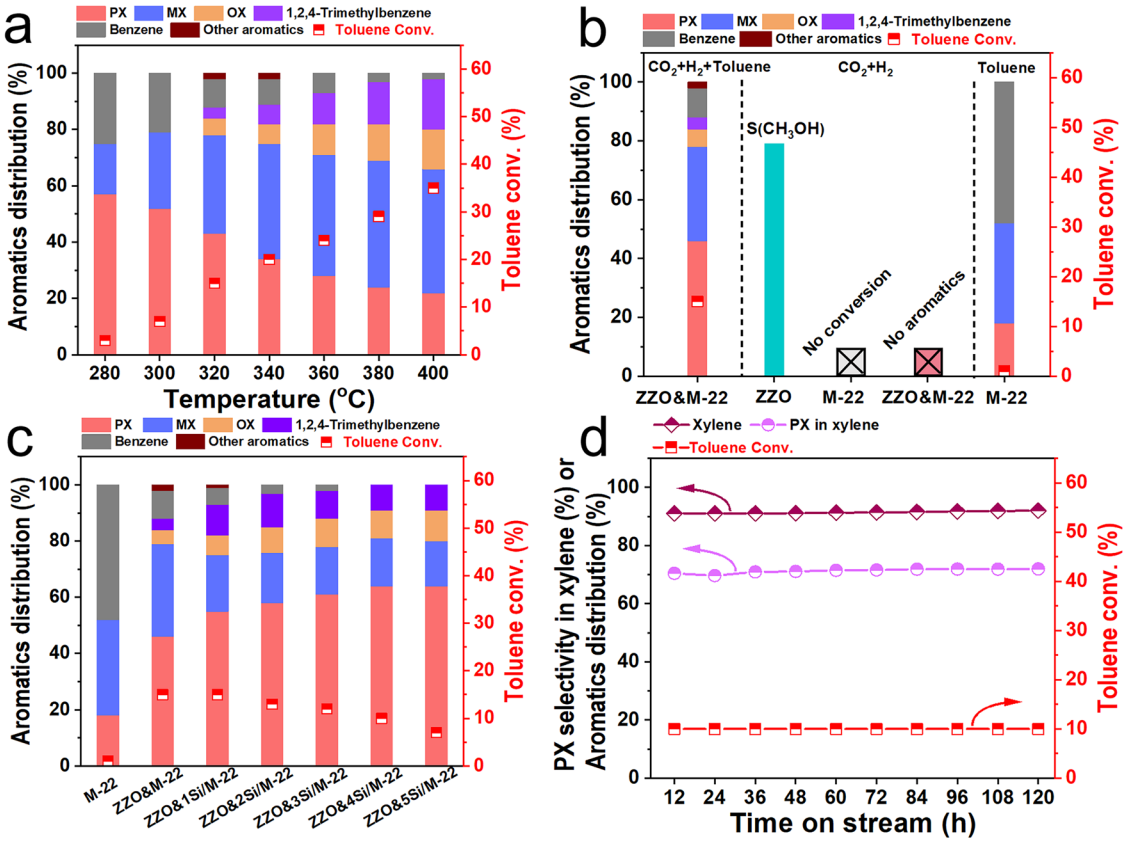

Fig. 1 | Catalytic Performance in CO_2 Hydrogenation. a The effect of reaction temperature. **b** CO_2 hydrogenation in the presence of toluene over ZZO & M-22; CO_2 hydrogenation over ZZO, M-22, ZZO & M-22 and toluene disproportionation over M-22. **c** Influence of M-22-modified times by TEOS on the aromatics distribution and toluene conversion. **d** The Stability test. Standard reaction conditions: 3 MPa, 320 °C, GHSV of a mixture gas ($CO_2/H_2/Ar$ = 24:72:4) = 12000 mL g^{-1} h^{-1}, and WHSV of toluene = 1 h^{-1}. When only toluene: 3.0 MPa, WHSV of toluene = 1 h^{-1}, GHSV of mixture gas ($CO_2/H_2/Ar$ = 24:72:4) = 12000 mL g^{-1} h^{-1}. The color shadings represent the selectivity, and the red square represents the conversion.

successful formation of a solid solution structure. The M-22 zeolite component displays well-defined nanosheet morphology, as observed in Fig. 2d. These crystalline sheets exhibit thicknesses of approximately 28 nm and lateral dimensions ranging from 300 to 500 nm. In the ZZO & M-22 tandem catalyst system, scanning electron microscopy (SEM) characterization reveals that ZZO nanoparticles are uniformly dispersed across the M-22 nanosheet surfaces (Fig. 2e). A critical observation from the high-resolution SEM image is the preservation of distinct structural features for both components, indicating that the interfacial interaction between ZZO and M-22 remains primarily physical rather than chemical. Additional structural validation is provided in Supplementary Fig. 3a, b, which present SEM images of the 4Si/M-22 modified sample. The morphology of M-22 nanosheets remains essentially unchanged after TEOS treatment, confirming that the structural integrity of the zeolite framework is maintained during the modification process. And the specific BET surface area, micropore area, external area and pore volume of M-22 all decreased, while the pore diameter remained almost unchanged. (Supplementary Table 2). This indicates that TEOS does not deposit extensively within the internal pores of the M-22, but predominantly at the entrances of all channels and on the external surface, thereby enhancing the shape selectivity of M-22.

Surface chemical properties of the tandem catalysts

CO_2 temperature-programmed desorption (CO_2-TPD) analysis reveals distinct adsorption behaviors between components (Supplementary Fig. 4a). The ZZO solid solution demonstrates sustained CO_2 adsorption up to 500 °C, while the zeolite component exhibits negligible CO_2 adsorption capacity. Quantitative evaluation of basic sites confirms that the physical integration of zeolite in the tandem catalyst exerts minimal influence on CO_2 adsorption performance of ZZO (Supplementary Table 3). The superior PX selectivity observed in ZZO & 4Si/M-22 tandem catalysts highlights the critical role of TEOS modification. This performance enhancement correlates with the decisive influence of zeolite acid properties (both quantity and type) on PX selectivity. To elucidate this relationship, comprehensive acid characterization was conducted using NH_3-TPD, pyridine Fourier-transform infrared (Py-FTIR) spectroscopy, ^{1}H MAS NMR, and ^{27}Al MAS NMR. NH_3-TPD profiles (Supplementary Fig. 4b) exhibit two characteristic desorption regions: weak acid sites (50–250 °C) and strong acid sites (250–500 °C). As shown in Supplementary Table 4, the total acid content of the ZZO & M-22 tandem catalyst closely matches the arithmetic sum of individual components, confirming that physical mixing preserves the intrinsic acidity of both ZZO and M-22.

Systematic investigation of acid evolution for M-22 under successive TEOS modifications reveals progressive acid suppression (Fig. 3a). Notably, both weak and strong acid contents stabilize after four modification cycles, indicating saturation of surface passivation. Py-FTIR analysis identifies characteristic bands at 1540 cm^{-1} (Brønsted acid sites) and 1440 cm^{-1} (Lewis acid sites), with quantitative analysis following established protocols (Fig. 3b)[25]. Supplementary Table 5 demonstrates a marked reduction in both acid types with increasing modifications, particularly the near-complete elimination of Brønsted acidity after four cycles. This evidences TEOS-mediated encapsulation of acid sites within external surface pockets of M-22. ^{1}H MAS NMR spectra (Fig. 3c) provide further validation of TEOS-induced acid

https://doi.org/10.1038/s41467-025-67695-4

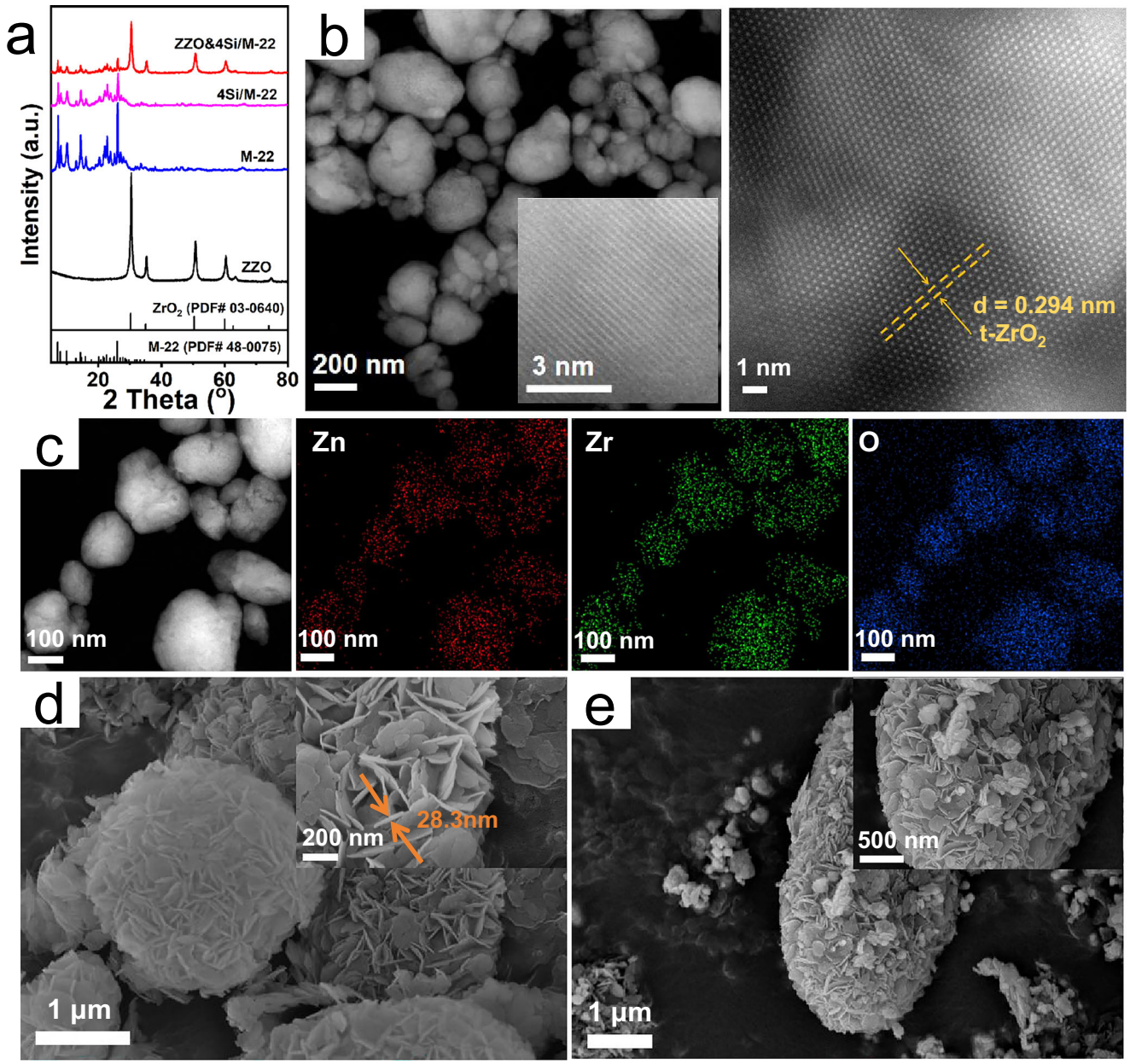

Fig. 2 | Structure characterization of the tandem catalysts. a X-ray diffraction patterns of ZZO, M-22, and ZZO & 4Si/M-22. **b** The TEM and Aberration-corrected HRTEM images of ZZO. **c** Aberration-corrected high-angle annular dark-field scanning TEM images and elemental distribution of Zn and Zr for ZZO. **d** SEM image of M-22. **e** SEM image of ZZO & M-22.

modulation. The diminishing signal at 1.8 ppm (assigned to external silanol groups, Si-OH[26]) and attenuated resonance at 3.9 ppm (bridging hydroxyls, Si(OH)Al[27,28]) correlate with modification cycles. Concurrent chemical shift variations in the 3.9 ppm band reinforce the role of TEOS in external surface acid passivation, as quantified in Supplementary Table 6.

Considering the intrinsic link between Brønsted acidity and framework aluminum (Al_F) in zeolites (Supplementary Fig. 5), ^{27}Al MAS NMR analysis was employed to probe Al speciation (Fig. 3d). Distinct resonances at 0 ppm (extra-framework Al_{EF}, 6-coordinated) and 56 ppm (framework Al_F, 4-coordinated) were identified[29]. Deconvolution of the 56 ppm band resolves three components: 50 ppm (T6 + T7 sites), 56 ppm (T1 + T3 + T4 + T5 + T8 sites), and 61 ppm (T2 sites)[30]. Structural analysis localizes T2 and T1 + T3 sites in supercages/surface pockets, T4 in inaccessible framework positions, T5 in sinusoidal channels with unstable and unfavorable for siting Al, and T8 in the sinusoidal channels connected to the bottom of the supercages, with thermodynamically stable bridging hydroxyls[31–33], with T6 + T7 residing on external surfaces[34]. Progressive TEOS modification induces three critical changes: gradual attenuation of the Al_{EF} signal at 0 ppm; systematic reduction of overall Al_F intensity at 56 ppm; selective disappearance of the 61ppm component (T2 supercage sites) upon deconvolution (Supplementary Table 7, Supplementary Fig. 6a).

These observations suggest TEOS not only passivates external surface pocket acid sites but also modulates supercage acidity. This aligns with literature demonstrating toluene disproportionation (a benzene-forming side reaction) predominantly occurs in MWW-type supercages[35,36]. Consistent with Fig. 1c, reduced benzene selectivity parallels TEOS-induced supercage deactivation. Complementary ^{27}Al MAS NMR analysis of precoked M-22 confirms analogous attenuation of 61 ppm signals (Supplementary Fig. 6b, c), validating efficacy of

https://doi.org/10.1038/s41467-025-67695-4

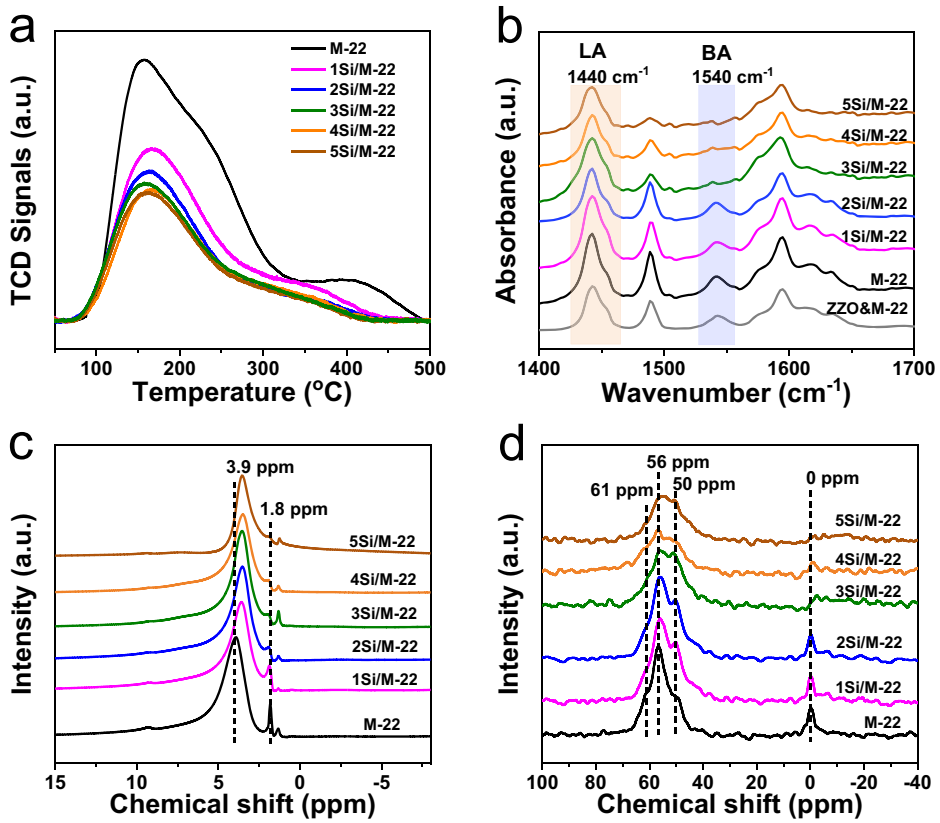

Fig. 3 | Surface chemical properties of the tandem catalysts. a NH_3-TPD of M-22 with different Si modification times. **b** Pyridine-FTIR results for M-22 with different Si modification times. **c** ^1H MAS NMR characterizations of M-22 with different Si modification time. **d** ^{27}Al MAS NMR characterizations of M-22 with different Si modification times. Lewis Acid (LA) and Brønsted acid (BA).

TEOS in suppressing toluene disproportionation through targeted acid site passivation.

Unraveling the key formaldehyde intermediates species and the reaction mechanism

The reaction mechanism was investigated through multiple complementary techniques. In situ DRIFTS analysis of ZZO during CO_2 hydrogenation revealed formate (HCOO*) and methoxy (H_3CO*) intermediates, with characteristic vibrations at 1595/1370 cm^{-1} (OCO stretching) and 2931/2824 cm^{-1} (C-H modes), respectively (Supplementary Fig. 7a). Isotopic substitution ($CO_2 + D_2$) caused rapid depletion of HCOO*/H_3CO* signals within 5 min, replaced by transient DCOO* (2165 cm^{-1}) and HD_2CO* (2050 cm^{-1}) species, confirming the formate pathway dominates CO_2 hydrogenation over ZZO (Supplementary Fig. 7b)[1]. Isotope-switching ($^{13}CO_2$) experiments confirmed CO_2 incorporation into products through 15 cm^{-1} redshift (2880 → 2865 cm^{-1}) in methyl C-H vibrations and intensified aromatic signals (Fig. 4a)[21,37,38]. Compared to ZZO, ZZO & 4Si/M-22 showed selective disappearance of H_3CO* species, while the HCOO* species still retain suggesting intermediate derived from formate species transfer to the zeolite component, thereby involving the formation of PX (Fig. 4b).

Quasi in situ ^{13}C NMR revealed surface species evolution (Fig. 4c): ZZO in $^{13}CO_2 + H_2$ showed formates (169 ppm), methoxy (52 ppm), and methanol (49 ppm)[39,40] while ZZO & 4Si/M-22 in $^{13}CO_2 + H_2 + C_7H_8$ exhibited depleted CH_xO signals alongside emerging xylene and trimethylbenzene signatures (20.9 ppm and 19.5 ppm)[41,42]. ^1H-^{13}C 2D heteronuclear correlation (HETCOR) NMR correlations confirmed these assignments formate (169/8.4 ppm), methoxy (52/3.7 ppm), and methanol (48/3.2 ppm) in ZZO (Fig. 4d), transitioning to PX and 1,2,4-trimethylbenzene signals (20.9/2.4 ppm and 19.5/1.84 ppm) in the tandem system (Fig. 4e). Collectively, these results demonstrate CH_xO* identified as the key intermediate enabling selective PX formation through spatial proximity effects in the tandem catalyst system, and the depletion of CH_xO species promotes formate conversion.

To further identify the CH_xO intermediates and their migration behavior from ZZO to MCM-22, controlled experiments were performed (Fig. 4f, 4g). Significantly, side product—specifically 2-(m-methylbenzyl)toluene (2MMBT), 4-(p-methylbenzyl)toluene (4PMBT), and 2-(p-methylbenzyl)toluene (2PMBT)—were detected with selectivity of 3% during CO_2 hydrogenation coupled with toluene over the ZZO & M-22 tandem catalyst (Fig. 4f, top panel; Supplementary Fig. 8a). This observation suggests that CH_2O species, generated from CO_2 hydrogenation, react with toluene, initially forming methylbenzyl alcohol intermediates. These intermediates then undergo further reactions with toluene to produce the observed side products. Crucially, when formaldehyde (CH_2O) was used as a methylating agent, replacing CO_2/H_2, identical side products were formed. In contrast, methanol, as a methylating agent, did not lead to the formation of these compounds. Furthermore, formaldehyde exhibited more favorable reaction kinetics compared to methanol, facilitating PX formation at lower temperatures and achieving higher PX selectivity (Supplementary Fig. 8b). In situ SVUV-PIMS analysis enabled the identification of key intermediates through their characteristic ionization thresholds (Fig. 4h, i): m/z = 30 (H_2CO, 10.88 eV) and m/z = 32 (CH_3OH, 10.85 eV), which are consistent with values reported in the literature[43,44]. These findings confirm that CH_2O* are generated over ZZO, and that formaldehyde—not methanol—acts as the alkylating agent formed from $CO_2 + H_2$ over the ZZO & M-22 tandem catalyst. Reaction kinetics further support the formation of CH_2O* species formed over ZZO from CO_2 hydrogenation, with methanol being produced over ZZO (Fig. 1b). To confirm that alkylation occurs exclusively over MCM-22 and not

https://doi.org/10.1038/s41467-025-67695-4

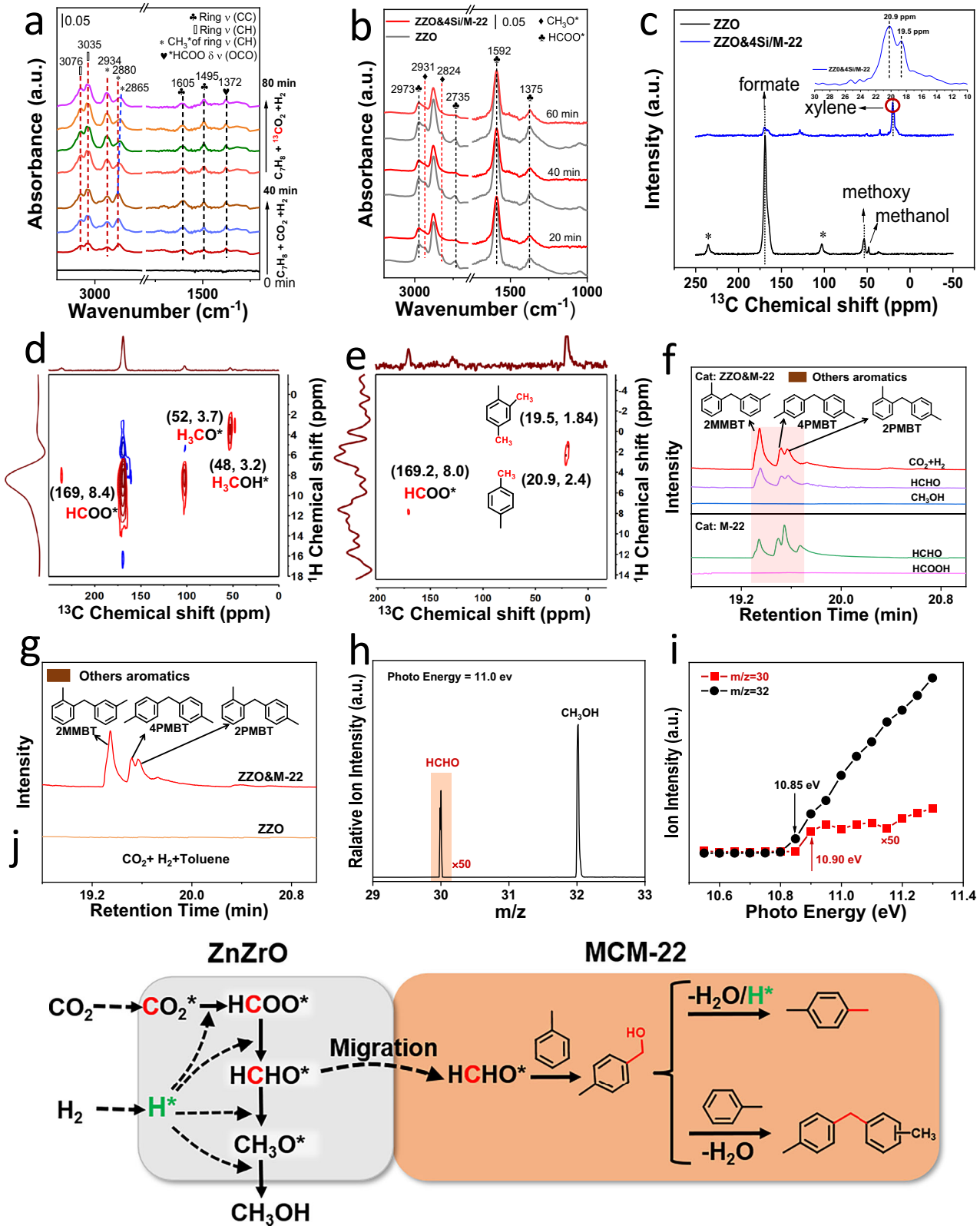

Fig. 4 | Surface species and the key formaldehyde intermediates derived from the reactions. a In situ DRIFTS spectra over the ZZO & 4Si/M-22 catalyst exposed to the stream of $C_7H_8 + CO_2 + H_2$ and subsequently switched to $C_7H_8 + {}^{13}CO_2 + H_2$. **b** In situ DRIFTS of $CO_2 + H_2$ over ZZO and ZZO & 4Si/M-22. **c** Quasi in situ ^{13}C CP MAS NMR experiment for $^{13}CO_2 + H_2$ on ZZO and $^{13}CO_2 + H_2 + C_7H_8$ on ZZO & 4Si/M-22. **d** Quasi in situ 2D ^{13}C-1H HETCOR MAS NMR experiment for $^{13}CO_2 + H_2$ on ZZO. **e** Quasi in situ 2D ^{13}C-1H HETCOR MAS NMR experiment for $^{13}CO_2 + H_2 + C_7H_8$ on ZZO & 4Si/M-22. Reaction conditions: 320 °C, 3 MPa, 30 min tube-sealing test. **f** The GC-MS chromatograms of the others aromatics in the products from alkylation of toluene with different alkylation reagents ($CO_2 + H_2$, formaldehyde and methanol) over the ZZO & M-22 and M-22 catalyst. **g** The GC-MS chromatograms of the others aromatics in the products from alkylation of toluene with $CO_2 + H_2$ over the ZZO & M-22 and ZZO catalyst. **h** In situ SVUV-PIMS detection of gas-phase products and **i** photoionization efficiency spectra of the signals at m/z = 30 and 32 over ZZO catalyst during $CO_2 + H_2$. (300 °C, 0.8 MPa, 9,000 mL g_{cat}^{-1} h^{-1} and $H_2/CO_2 = 3/1$). **j** The reaction pathway over the ZZO & M-22 catalyst.

https://doi.org/10.1038/s41467-025-67695-4

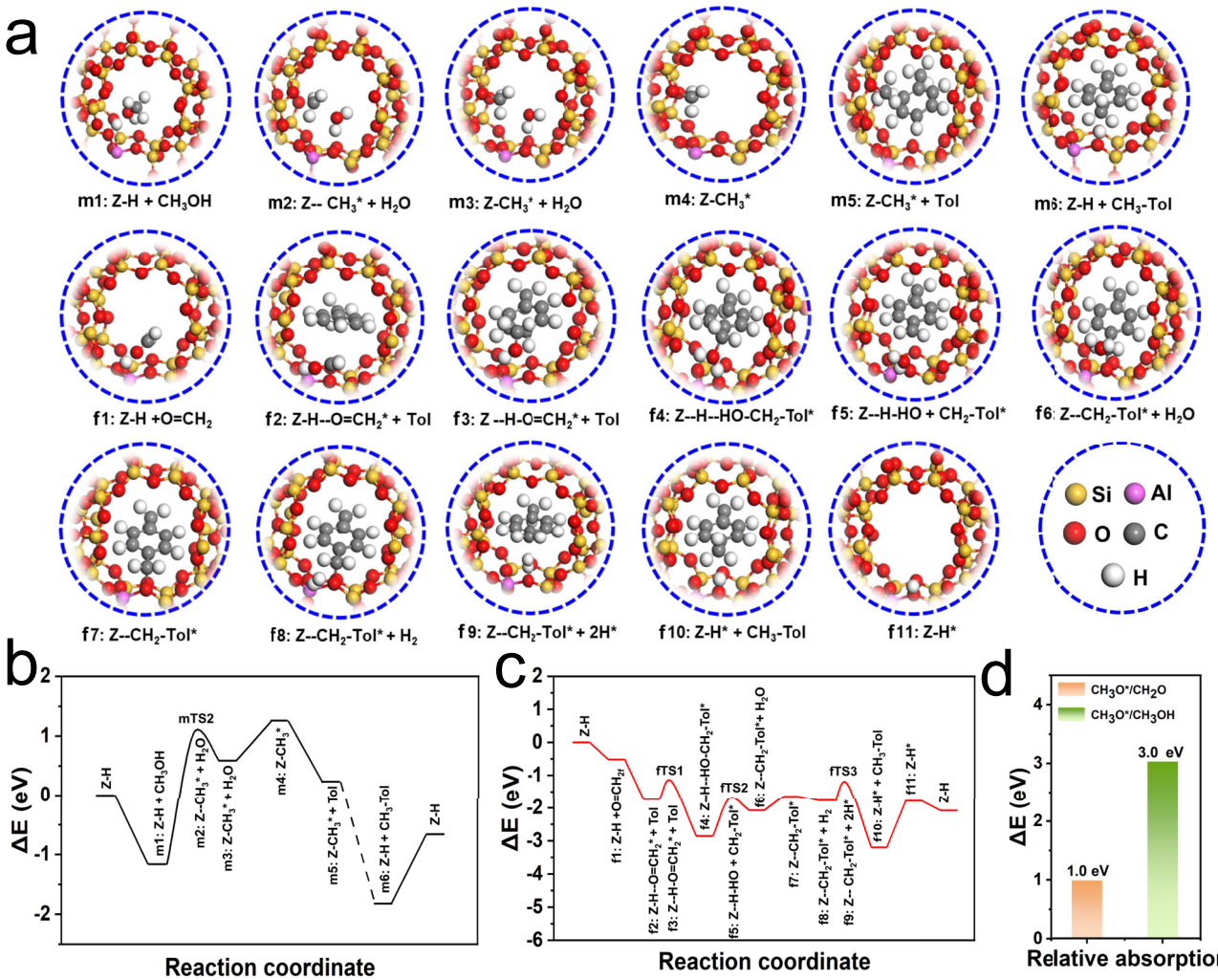

Fig. 5 | DFT calculations on the reaction pathway. a Optimized geometries of all reaction intermediates and transition states. Reaction Gibbs free energy diagram: **b** Methanol reacting with toluene over M-22 zeolite, **c** CH_2O^* reacting with toluene on M-22 zeolite. **d** The initial adsorption energy of CH_3O^* relative to CH_2O^* and CH_3OH in M-22.

ZZO, the reaction of $CO_2 + H_2$ with toluene was carried out over isolated ZZO catalyst (Supplementary Fig. 9). This experiment unequivocally demonstrated that alkylation requires the presence of the MCM-22 component. These results indicate the CH_2O^* species, formed over ZZO, can migrate to M-22 site to contribute to the formation of PX.

Based on the results presented above, the following reaction pathway is proposed, as illustrated in Fig. 4j. Initially, CO_2 and H_2 are adsorbed and activated on the ZZO component, leading to the formation of HCOO* species. These HCOO* species then undergo hydrogenation to produce CH_2O^* intermediates. The CH_2O^* intermediates subsequently migrate to the MCM-22 zeolite, where they react with toluene to form methylbenzyl alcohol, with para-methylbenzyl alcohol being the dominant product. The para-methylbenzyl alcohol then primarily undergoes dehydration, followed by hydrogenation, to yield the target product, PX. In parallel, some of the methylbenzyl alcohol can react with an additional toluene molecule, resulting in the formation of side products—2MMBT, 4PMBT, and 2PMBT.

DFT calculations on the reaction pathway

The experimental findings collectively suggest that CH_2O^* serves as the critical intermediate enabling kinetic coupling between the ZZO and M-22 components in the tandem catalytic system. To validate this hypothesis at the molecular level, density functional theory (DFT) calculations were conducted to compare three potential intermediates–CH_2O^*, CH_3O^*, and CH_3OH in their ability to migrate from ZZO into sinusoidal channels of M-22. For the methanol-mediated pathway (Fig. 5a m1-m6), the mechanism initiates with methanol adsorption at the Brønsted acid site in the T8 position of sinusoidal channel in M-22 (Fig. 5a). Subsequent dehydration through transition state mTS2 generates a methyl group (CH_3) and water, requiring a substantial activation barrier of 2.05 eV (Fig. 5b). Following water desorption (Fig. 5a m4), toluene enters the framework where the CH_3 group attacks the para-carbon of the aromatic ring (Fig. 5a m5), ultimately yielding desorbed PX (Fig. 5a m6).

In contrast, the CH_2O^*–mediated pathway demonstrates superior thermodynamic feasibility (Fig. 5a f1-f11). Initial adsorption of CH_2O^* at the T8 Brønsted site (Fig. 5a f1) is followed by protonation to form a hydroxymethyl cation (CH_2OH^*) (Fig. 5c f2). Concurrent toluene ingress enables para-carbon attack via transition state fTS1 (Fig. 5c), forming H--HO-CH_2-Tol* (Fig. 5c f3-f4). The rate-determining step involves C-O bond cleavage through transition state fTS2 (1.19 eV barrier) (Fig. 5c f5), yielding CH_2-Tol* and water (Fig. 5c f6). Subsequent hydrogen transfer from surface H* species (Fig. 5c f8) via transition state fTS3 (Fig. 5c f9) generates CH_3-Tol*, culminating in PX desorption (Fig. 5c f11). Notably, CH_3O^* exhibits substantially higher adsorption energies compared to both CH_2O^* (+1.0 eV) and CH_3OH (+3.0 eV)

(Fig. 5d), rendering it thermodynamically unfavorable for alkylation within M-22. The maximum activation barrier of CH_2O*-mediated pathway (1.19 eV) remains significantly lower than that of methanol barrier (2.05 eV), conclusively identifying CH_2O* as the kinetically favored intermediate.

In summary, this work demonstrates a tandem catalytic strategy for direct PX synthesis via CO_2 hydrogenation coupled with toluene methylation using a ZZO & M-22 system. Compartmentalized catalysis enables synergy: ZZO preferentially activates CO_2/H_2, while M-22 channels mediate C–C coupling via CH_2O* intermediates. This approach overcomes thermodynamic constraints of conventional toluene methylation, achieving 91% xylene selectivity (70.4% PX/xylene) at 10.3% toluene conversion. TEOS modification of M-22 is critical, passivating supercage Brønsted acid sites (Si(OH)Al) via TEOS deposition to suppress disproportionation side reactions. Mechanistically, CH_2O* intermediates kinetically couple CO_2 activation and alkylation, bypassing methanol dehydration. Controlled diffusion of CH_2O* from ZZO to M-22 optimizes thermodynamic-kinetic balance, facilitating confined electrophilic para-methylation. This establishes a paradigm for tandem catalyst design through zeolite architecture engineering, where precise intermediate dimension/configurational control governs selectivity. The strategy offers an efficient CO_2 valorization route and a carbon recycling alternative to conventional PX production, underscoring structure-directed catalysis in bridging CO_2 utilization with aromatics synthesis.

Methods

Materials

$Zn(NO_3)_2 \cdot 6H_2O$ were purchased Sinopharm (China), $(NH_4)_2CO_3$, m-xylene (99%), toluene (99.9%) and $Zr(NO_3)_4 \cdot 5H_2O$, tetraethylorthosilicate (TEOS, 99.98%) and n-hexane (99%) were obtained from Macklin, $CO_2/H_2/Ar$ [24/72/4(v/v/v)], H_2 (99.99%) and Ar (99.99%) were obtained from Lanzhou Yulong Gas Co., Ltd. HMCM-22 (Si/Al=15) were obtained from Nankai Catalysts.

Preparation of catalysts

The ZnZrO catalyst that doped 20% ZnO (Zn/ (Zn + Zr) molar ratio) was prepared as follows. 14.9 g of Zn $(NO_3)_2 \cdot 6H_2O$ and 8.6 g of Zr $(NO_3)_4 \cdot 5H_2O$ were dissolved in a flask by using 400 mL of deionized water, then the 250 mL aqueous solution of $(NH_4)_2CO_3$ (43.2 g) as precipitant was dropwise added into the aforementioned solution under vigorous stirring at 70 °C to form a precipitate. The obtained suspension was continuously stirred for 4 h at 70 °C, followed by cooling down to room temperature and filtering. The precipitate was washed three times with deionized water, dried at 110 °C for 4 h, and calcined at 500 °C in static air for 3 h.

Si/M-22 zeolite was prepared by tetraethoxysilane (TEOS) modification. Typically, the steps to modify the M-22 once were to immerse 1 g M-22 into the mix solution of 1 g TEOS and 20 ml of n-hexane for 4 h; after that, organic solvent was removed by evaporation at 80 °C and the powder was dried overnight at 110 °C, followed by calcination at 550 °C for 4 h in air. While the above steps were repeated, a new symbol of nSi/M-22 (n means the number of repetitions) was used. After repeating the procedure above for four times, the 4Si/M-22 was obtained. The tandem catalyst was typically prepared by physical mixing. The weight ratio of oxides and zeolites was 1:1. For preparation of tandem catalyst ZZO & M-22, ZZO and M-22 were grinded in an agate mortar for 5 min, pressed under 10 MPa and granulated into the required size in the range of 40-80 mesh.

M-22 with the pre-coked supercages, denoted as pre-coked M-22 was prepared following the procedure: M-22 was pretreated at 500 °C for 2 h and then cooled down to 350 °C under Ar flow (100 mL min^{-1}). Subsequently, the transformation of m-xylene (99%) was carried out at 350 °C, atmospheric pressure and 8 h^{-1} of m-xylene WHSV with Ar flow (40 mL min^{-1}) for 12 h, to form pre-coked M-22.

Catalyst evaluation

Catalytic performance was evaluated on a high-pressure fixed-bed reactor equipped with a quartz sample tube. Typically, 0.52 g catalyst (40-80 mesh) were loaded into the quartz sample tube without mixed quartz sand. Before evaluating the catalytical performances, raised to the specified temperature under the protection of argon. For the investigation of toluene methylated with CO_2 and H_2, a mixture gas of $CO_2/H_2/Ar$ [24/72/4(v/v/v)] was induced into a quartz sample tube, and then toluene was carried into reaction tube (90 °C) at a constant flow rate by using a piston pump. The reaction was conducted at 320 °C and 3.0 MPa, with a GHSV of 12,000 mL g^{-1} h^{-1} and a toluene weight hourly space velocity (WHSV) of 1 h^{-1}, and the data were collected at the reaction time of 12 h. For the contrast experiment of toluene methylated with methanol/Formaldehyde (s-Trioxane), a mixed solution of C_7H_8/CH_3OH or HCHO [5/1 (mol/mol)] was pumped into reaction tube with a toluene WHSV of 1 h^{-1} at 320 °C /260 320 °C and 3.0 MPa, while 12,000 mL g^{-1} h^{-1}, H_2/Ar was used as a carry gas simultaneously. In the quantitative analysis, we use diphenyl as an internal standard to determine the C balance, and the C balance was above 96%. The liquid products were analyzed by using the gas chromatography equipped with CBX-WAX columns to analyze aromatics, the conversion of toluene and production selectivity was calculated as follows:

$$Conv.(\%) = \frac{\sum n_i}{n^{in}_{toulene}} \times 100 \quad (1)$$

$$Sel(\%) = \frac{n_i}{\sum n_i} \times 100 \quad (2)$$

Where n_i is the molar amount at the outlet of the individual aromatic product $_i$.

Catalyst characterization

The XRD analysis was performed using a Philips PW1050/81 diffractometer equipped with a CuKα radiation source (λ = 1.5418 Å). The instrument was operated in Bragg-Brentano geometry at 40 kV and 30 mA.

The specific surface area was calculated using the Brunauer-Emmett-Teller (BET) method. The textural properties of the samples, including specific surface area and pore size distribution, were characterized by N_2 physisorption using a MicrotracBEL BELSORP-mini II analyzer. Prior to analysis, approximately 0.2 g of each catalyst was subjected to degassing at 300 °C for 2 h.

The microstructural and elemental composition of the catalysts were characterized by aberration-corrected HAADF-STEM and STEM-EDX mapping, respectively, using an FEI Cubed Titan G2 60-300 microscope at an accelerating voltage of 300 kV. Morphological analysis was performed by scanning electron microscopy (SEM) on a Thermo Fisher Scientific Apreo S instrument. The SEM specifications were as follows: electron gun: field emission (FEG); accelerating voltage: 30–200 kV.

CO_2 and NH_3 temperature-programmed desorption (TPD) experiments were conducted using a Micromeritics ASAP 2920 system. Approximately 0.1 g of catalyst, loaded in a quartz reactor, was first pretreated at 500 °C under Ar flow for 3 h and subsequently cooled to 50 °C. The sample was then saturated with a flow of either 10 vol% CO_2/He or 10 vol% NH_3/He (50 mL min^{-1}) for 1 h at this temperature. Subsequently, the flow was switched to pure He for 1 h at 50 °C to purge physically adsorbed molecules. After stabilizing the baseline, the temperature was ramped to 700 °C at a rate of 10 °C min^{-1} under He flow, and the desorption signal was monitored by a thermal conductivity detector (TCD).

In-situ DRIFT spectra of surface species formed from the $CO_2/^{13}CO_2 + H_2/D_2$ reaction. Prior to the experiment, the samples were

heated to 450 °C for 2 h under an Ar atmosphere to remove any water contained in the cell and on the catalyst surface. In situ DRIFT spectra of surface species over ZZO from $CO_2 + H_2$ and subsequently switched to D_2. Reaction conditions: ZZO, 0.1 MPa, 320 °C, 30 mL min^{-1} $CO_2 + H_2$, D_2 10 mL min^{-1}. In situ DRIFT spectra of surface species over ZZO & 4Si/M-22, 30 ml/min CO_2 + 10 mL min^{-1} H_2 +toluene, subsequently switched to $^{13}CO_2$ was injected into the cell, and infrared spectrum information of the catalyst surface and species was collected.

FTIR spectra of pyridine was performed for both M-22 and nSi/M-22. The sample (about 30 mg) was pressed into a wafer, and then treated under vacuum at 400 °C for 1 h. After cooling to 50 °C, pyridine was introduced to the transmission cell until saturation. Then, the signal vs. the reference signal was recorded at 150 °C until the signal unchanged.

Magic angle spinning (MAS) nuclear magnetic resonance (NMR) spectra of ^{1}H and ^{27}Al were collected on a Bruker Avance III 600 MHz Wide Bore spectrometer operating at a magnetic field of 14.1 T, 4 mm dural-channel probe; the rotate speed of samples is 10.0 kHz; The chemical shifts for ^{27}Al MAS NMR spectra were referenced to the aqueous solution of $Al(NO_3)_3$ (0 ppm), respectively. The chemical shifts for ^{1}H MAS NMR spectra were referenced to tetramethylsilane (TMS). Quantitative ^{1}H MAS NMR measurement was performed by comparing the signal area of the zeolite sample under study with that of adamantine as an external standard.

Quasi in situ^{13}C CP MAS NMR experiment and Quasi in situ 2D ^{13}C-^{1}H HETCOR MAS NMR experiment are carried out as follows: the basic experimental device is a home-built high-pressure fixed-bed catalytic reactor. Standard reaction conditions: 3 MPa, 320 °C, 10 mL min^{-1} H_2 + 60 mL min^{-1} $^{13}CO_2$. The reactor was quickly immersed into liquid nitrogen to quench the reaction, so that highly reactive intermediates on the catalysts can be capture. Subsequently, the reactor was sealed, after waiting for recovery to room temperature, and further transferred into 4 mm rotor for further NMR experiment.

In situ SVUV-PIMS experiments were carried out beamline BL03U at the National Synchrotron Radiation Laboratory, Hefei, P.R. China. This technique is employed for the detection of oxygen-containing intermediates during the CO_2 hydrogenation process. The photoionization efficiency spectra were collected for 300 s in the energy range of 10.5-11.3 eV with a step of 0.05 eV. Reaction conditions: the ZnZrO catalyst (0.5 g); reaction gas (H_2/CO_2 = 3/1), at 300 °C, 0.8 MPa, GHSV = 12,000 mL g_{cat}^{-1} h^{-1}.

Data availability

All data needed to support the findings of this study are included in the main text or in the Supplementary Information. Data are available from the corresponding authors upon request.

References

1. Wang, J. et al. A highly selective and stable ZnO-ZrO_2 solid solution catalyst for CO_2 hydrogenation to methanol. *Sci. Adv.* **3**, e1701290 (2017).
2. Wang, J. et al. High-Performance M_aZrO_x (Ma= Cd, Ga) Solid-Solution Catalysts for CO_2 Hydrogenation to Methanol. *ACS Catal* **9**, 10253–10259 (2019).
3. Ma, Z. Q. et al. Development of Tandem Catalysts for CO_2 Hydrogenation to Olefins. *ACS Catal* **9**, 2639–2656 (2019).
4. Li, Z. L. et al. Highly Selective Conversion of Carbon Dioxide to Lower Olefins. *ACS Catal* **7**, 8544–8548 (2017).
5. Xu, Y. et al. Highly Selective Olefin Production from CO_2 Hydrogenation on Iron Catalysts: A Subtle Synergy between Manganese and Sodium Additives. *Angew. Chem. Int. Ed.* **59**, 21736–21744 (2020).
6. Yang, H. Y. et al. Selective synthesis of olefins via CO_2 hydrogenation over transition-metal-doped iron-based catalysts. *Appl. Catal. B Environ. Energy* **321**, 122050 (2023).
7. Ni, Y. M. et al. Selective conversion of CO_2 and H_2 into aromatics. *Nat. Commun.* **9**, 3457 (2018).
8. Wang, Y. et al. Rationally Designing Bifunctional Catalysts as an Efficient Strategy to Boost CO_2 Hydrogenation Producing Value-Added Aromatics. *ACS Catal* **9**, 895–901 (2019).
9. Li, Z. L. et al. Highly Selective Conversion of Carbon Dioxide to Aromatics over Tandem Catalysts. *Joule* **3**, 570–583 (2019).
10. Ahn, J. H. et al. Methanol Usage in Toluene Methylation with Medium and Large Pore Zeolites. *ACS Catal* **3**, 817–825 (2013).
11. Bi, Y. et al. Improved Selectivity toward Light Olefins in the Reaction of Toluene with Methanol Over the Modified HZSM-5 Catalyst. *ChemCatChem* **6**, 713–718 (2014).
12. Liu, X. L. et al. Selective transformation of carbon dioxide into lower olefins with a bifunctional catalyst composed of $ZnGa_2O_4$ and SAPO-34. *Chem. Commun.* **54**, 140–143 (2018).
13. Gao, P. et al. Direct Production of Lower Olefins from CO_2 Conversion via Bifunctional Catalysis. *ACS Catal* **8**, 571–578 (2018).
14. Chen, S. Y. et al. Hydrogenation of CO_2 to Light Olefins over $ZnZrO_x$/SSZ-13. *Angew. Chem. Int. Ed.* **63**, e202316874 (2024).
15. Zhou, C. et al. Highly Active ZnO-ZrO_2 Aerogels Integrated with H-ZSM-5 for Aromatics Synthesis from Carbon Dioxide. *ACS Catal* **10**, 302–310 (2020).
16. Zhang, J. F. et al. Hydrogenation of CO_2 into aromatics over a $ZnCrO_x$-zeolite composite catalyst. *Chem. Commun.* **55**, 973–976 (2019).
17. Miao, D. et al. Selective synthesis of para-xylene and light olefins from CO_2/H_2 in the presence of toluene. *Catal. Sci. Technol.* **11**, 4521–4528 (2021).
18. Shang, X. et al. Regulating anisotropic diffusion in zeolite for reinforced para-xylene synthesis via CO_2 hydrogenation in the presence of toluene. *Appl. Catal. B Environ. Energy* **359**, 124523 (2024).
19. Hong, B. et al. Low-pressure CO_2 hydrogenation coupled with toluene methylation to para-xylene using atomic Pd-doped $ZnZrO_x$-HZSM-5. *Appl. Catal. B Environ. Energy* **361**, 124606 (2025).
20. Tuo, J. et al. Shape-selective synthesis of para-xylene through tandem CO_2 hydrogenation and toluene methylation over $ZnCeZrO_x$/MCM-22 catalyst. *Chin. J. Catal.* **73**, 174–185 (2025).
21. Zuo, J. C. et al. Selective methylation of toluene using CO_2 and H_2 to p-xylene. *Sci. Adv.* **6**, eaba5433 (2020).
22. Xiao, Z. K. et al. Designing a bifunctional $ZrCuO_x$/HZSM-5 catalyst for selective methylation of toluene with carbon dioxide to para-xylene. *Fuel* **319**, 123848 (2022).
23. Zhu, Z. R. et al. Catalytic performance of MCM-22 zeolite for alkylation of toluene with methanol. *Catal. Today* **93**, 321–325 (2004).
24. Parmar, D. et al. Spatiotemporal Coke Coupling Enhances para-Xylene Selectivity in Highly Stable MCM-22 Catalysts. *J. Am. Chem. Soc.* **144**, 7861–7870 (2022).
25. Madeira, F. F. et al. Ethanol transformation into hydrocarbons on ZSM-5 zeolites: Influence of Si/Al ratio on catalytic performances and deactivation rate. Study of the radical species role. *Appl. Catal. A Gen.* **443**, 171–180 (2012).
26. Hunger, M. et al. Multinuclear solid-state nmr investigation of zeolite MCM-22. *Zeolites* **15**, 188–192 (1995).
27. Ma, D. et al. An investigation of the roles of surface aluminum and acid sites in the zeolite MCM-22. *Chem. Eur. J.* **8**, 162–170 (2002).
28. Ma, D. et al. MAS MMR studies on the dealumination of Zeolite MCM-22. *J. Phys. Chem. B* **105**, 1770–1779 (2001).
29. Corma, A. et al. Infrared spectroscopy, thermosprogrammed desorption, and nuclear magnetic resonance study of the acidity, structure, and stability of zeolite MCM-22. *Zeolites* **15**, 576–582 (1995).

30. Kennedy, G. J. et al. Multinuclear MAS NMR studies of zeolites MCM-22 and MCM-49. *Catal. Today* **49**, 385–399 (1999).
31. Zhou, D. H. et al. DFT studies on the location and acid strength of Bronsted acid sites in MCM-22 zeolite. *J. Mol. Catal. A Chem.* **244**, 11–19 (2006).
32. Sastre, G. et al. Preferential siting of bridging hydroxyls and their different acid strengths in the two-channel system of MCM-22 zeolite. *J. Phys. Chem. B* **104**, 4349–4435 (2000).
33. Li, Y. et al. A DFT study on the distributions of Al and Bronsted acid sites in zeolite MCM-22. *J. Mol. Catal. A Chem.* **338**, 24–32 (2011).
34. Mériaudeau, P. et al. On the localization of tetrahedral aluminum in MCM-22 zeolite. *Catal. Lett.* **61**, 89–92 (1999).
35. Wu, P. et al. Selective formation of p-xylene with disproportionation of toluene over MCM-22 catalysts. *Micropor. Mesopor. Mat.* **22**, 343–356 (1998).
36. Laforge, S. et al. m-Xylene transformation over H-MCM-22 zeolite 1: Mechanisms and location of the reactions. *J. Catal.* **220**, 92–103 (2003).
37. Muller, G. et al. Infrared microscopic study of sorption and diffusion of toluene in ZSM-5. *J. Phys. Chem.* **98**, 7436–7439 (1994).
38. El-Sabbagh, O. I. et al. Synthesis and antiviral activity of new pyrazole and thiazole derivatives. *Eur. J. Med. Chem.* **44**, 3746–3753 (2009).
39. Larmier, K. et al. CO_2-to-Methanol Hydrogenation on Zirconia-Supported Copper Nanoparticles: Reaction Intermediates and the Role of the Metal-Support Interface. *Angew. Chem. Int. Ed.* **56**, 2318–2323 (2017).
40. Ji, Y. et al. Oxygenate-based routes regulate syngas conversion over oxide-zeolite bifunctional catalysts. *Nat. Catal.* **5**, 594–604 (2022).
41. Wang, C. et al. Unraveling Spatially Dependent Hydrophilicity and Reactivity of Confined Carbocation Intermediates during Methanol Conversion over ZSM-5 Zeolite. *J. Am. Chem. Soc.* **146**, 8688–8696 (2024).
42. Shang, X. et al. Xylene Synthesis Through Tandem CO_2 hydrogenation and toluene methylation over a composite ZnZrO Zeolite Catalyst. *Angew. Chem. Int. Ed.* **62**, e202309377 (2023).
43. Yang, H. Y. et al. Tuning the selectivity of CO_2 hydrogenation to alcohols by crystal structure engineering. *Chem* **10**, 2245–2265 (2024).
44. Hu, J. T. et al. Sulfur vacancy-rich MoS_2 as a catalyst for the hydrogenation of CO_2 to methanol. *Nat. Catal.* **4**, 242–250 (2021).

Acknowledgements

This work thank beamline BL04B at the National Synchrotron Radiation Laboratory, Hefei, P.R. China, for the beam time and assistance with experiments. This work was supported by the National Key R & D Program of China (2023YFB4104501) and the National Natural Science Foundation of China (grant nos. 223B2204 and U24A20493).

Author contributions

J.T. and Y.X. contributed equally. J.T. conceived and conducted the experiments, and analyzed data; Y.X. conducted the DFT calculations; J.C., J.Z., H.W., F.R., J.Y., C.H., and H.Y. offered the help in the experiments and data analysis; C.L. conducted the in situ SVUV-PIMS experiments. The manuscript was written by Z.L.; Z.L. and C.L. proposed the project, analyzed data and revised the manuscript.

Competing interests

The authors declare no competing interests.

Additional information

Supplementary information The online version contains supplementary material available at https://doi.org/10.1038/s41467-025-67695-4.

Correspondence and requests for materials should be addressed to Zelong Li or Can Li.

Peer review information *Nature Communications* thanks the anonymous reviewers for their contribution to the peer review of this work. A peer review file is available.